~~Characterization~~ Aerogeophysical characterization of Titan Dome, East Antarctica, and potential as an ice core target

Lucas H. Beem[1], Duncan A. Young[2], Jamin S. Greenbaum[2], Donald D. Blankenship[2], Marie G. P. Cavitte[3], Jingxue Guo[4], and Sun Bo[4]

[1]Department of Earth Sciences, Montana State University, Bozeman, MT 59717, USA
[2]Institute for Geophysics, University of Texas at Austin, Austin, TX 78758, USA
[3]Université catholique de Louvain, Earth and Life Institute, Georges Lemaître Centre for Earth and Climate Research, Place LouisPasteur, B-1348 Louvain-la-Neuve, Belgium
[4]Polar Research Institute of China, Shanghai 200136, China

Correspondence: Lucas Beem (lucas.beem@montana.edu)

Abstract. ~~Titan Dome is~~ Based on sparse data, Titan Dome, located about 200 km from the South Pole ~~along the 180° meridian~~ within the East Antarctic Ice Sheet~~. Based on sparse data, it is a region that is~~ , has been identified as having a higher probability of containing ice that would capture the middle Pleistocene transition (1.25 to 0.7 Ma)~~as a paleoclimate proxy. New aerial geophysical observations~~ . New aero-geophysical observations (radar and laser altimetry) collected over Titan Dome were used to characterize the region ~~and~~ (e.g. geometry, internal structure, bed reflectivity, and flow history) and assess its suitability as a paleoclimate ice core site. The radar coupled with an available ice core ~~age model~~ chronology enabled the tracing of ~~isochronal layers~~ dated internal reflecting horizons throughout the region which also served as constraints on ~~basal ice~~ basal-ice age modeling. The results of the survey revealed new basal topographic detail ~~, constrained the~~ and better constrains the ice topographical location of Titan Dome, which differs between community datasets~~, and suggests that the basal ice beneath~~ . Titan Dome is ~~too young~~ not expected to be relevant to the study of the middle Pleistocene transition due to a combination of past fast flow dynamics, the basal ice likely being too young, and the temporal resolution too coarse if 1 Ma ice were to exist.

1 Introduction

The ice domes and ridges of Antarctica hold the best stratigraphically ordered records of past ice sheet and climate evolution~~and there~~ . There is an ongoing international effort ~~(Fischer et al., 2013)~~ (e.g. Fischer et al., 2013; Passalacqua et al., 2018) to find suitable ice core drilling sites that will have an interpretable climate record that spans the middle Pleistocene transition, dated to between 1.25 Ma and 0.7 Ma (Clark et al., 2006). During this period, marine oxygen isotope records indicate a transition in major ice volume and climate cycles from a predominately ∼41,000 year obliquity driven periodicity to a ∼100,000 ~~periodicity.~~

~~An ice core's proxies, e.g.~~ year periodicity. The trapped atmospheric gases and ~~ice isotopic chemistry , hold~~ isotopic chemistry of ice cores are proxy records of atmospheric and ice sheet configuration that are key to understanding this transition and climate dynamics more generally.

Identifying ~~suitable coring locations~~ coring locations to study the middle Pleistocene transition has primarily been the result of ~~ice dynamic and ice temperature~~ modeling efforts that find regions ~~where ice is dynamically and thermodynamically stable enough~~ that have ice dynamic and thermodynamic stability suitable to allow for both ~~ice survival for~~ 1.5 Ma of ice survival and the existence of a ~~simple chronological record~~well-preserved ice stratigraphy. One such effort used a one-dimensional thermodynamic model to find where the bed is sufficiently cold to prevent present-day basal melting (Van Liefferinge and Pattyn, 2013). With their model results and the additional criteria of present-day slow flow of less than 2 m yr^{-1} and ice thickness greater than 2000 m~~(Fischer et al., 2013)~~ , they identified regions with increased likelihood for the recovery of ~~a suitably old ice core were defined (fig~~an ice core dating to the middle Pleistocene transition (Fig. 1). Follow on work (Van Liefferinge et al., 2018), used updated methodology and included additional processes, such as parametrization that allows for accumulation rate variability, to refine the boundaries of promising regions. For the regions near Titan Dome (Fig 1, the boundaries are generally consistent.

Not all relevant processes and conditions have been explicitly considered in site determination efforts. Additional ~~processes~~ considerations that might impact the existence or quality of the desired ice core include past ice flow reorganization and/or ice divide migration ~~(Beem et al., 2017)~~(Beem et al., 2017; Winter et al., 2018), subglacial groundwater flow (Gooch et al., 2016), ~~accumulation rate variability,~~ ice surface wind erosion, heterogenous geothermal flux ~~(Jordan et al., 2018). Modeling to enable core site determination has also been hindered by poorly constrained and increasingly divergent estimates of continental scale geothermal flux variability beneath the Antarctic Ice Sheet (Shapiro and Ritzwoller, 2004; Maule et al., 2005; Purucker, 2013; An et al., 20~~ (e.g. Jordan et al., 2018), and minimum age resolution of ∼10 kyr m^{-1} of ice (Fischer et al., 2013). Without geophysical observations, and in some cases direct access, the presence or significance of these processes cannot be determined. Aerial and ground geophysical surveys have occurred for some high probability coring targets, including at Dome C of East Antarctica (Young et al., 2017). Planning for drilling at Dome C is ~~a leading contender for successful extraction of a sufficiently old ice core due to~~ proceeding based on the characterization of the region (Young et al., 2017), the existence of a proximal ∼800,000 year old EPICA ice core (Augustin et al., 2004), and promising ice age modeling (Parrenin et al., 2017). However, finding additional targets remains of interest to enable ~~the possibility of~~ multiple correlatable cores and the examination of spatial heterogeneity in climate processes.

Titan Dome, located ~~about~~ approximately 200 km along the ~~∼180~~-170°E meridian from South Pole, is a region that was previously identified as a contender for ~~possible~~ the existence of 1.5 million year old ice ~~(Van Liefferinge and Pattyn, 2013)~~ (Van Liefferinge and Pattyn, 2013; Van Liefferinge et al., 2018). In 2016 and 2017, a partnership between the University of Texas Institute for Geophysics and the Polar Research Institute of China surveyed the South Pole Corridor (SPC) grid ~~over the region~~ to evaluate the location as an ice core target. The existence of ~~an ice core age model at South Pole (Casey et al., 2014)~~the South Pole Ice Core chronology (Casey et al., 2014; Winski et al., 2019), plus previously collected aerial-geophysical surveys in the region ~~(Carter et al., 2007; Beem et al., 2017; Jordan et al., 2018) helps propagate englacial reflector ages~~ (Carter et al., 2007)

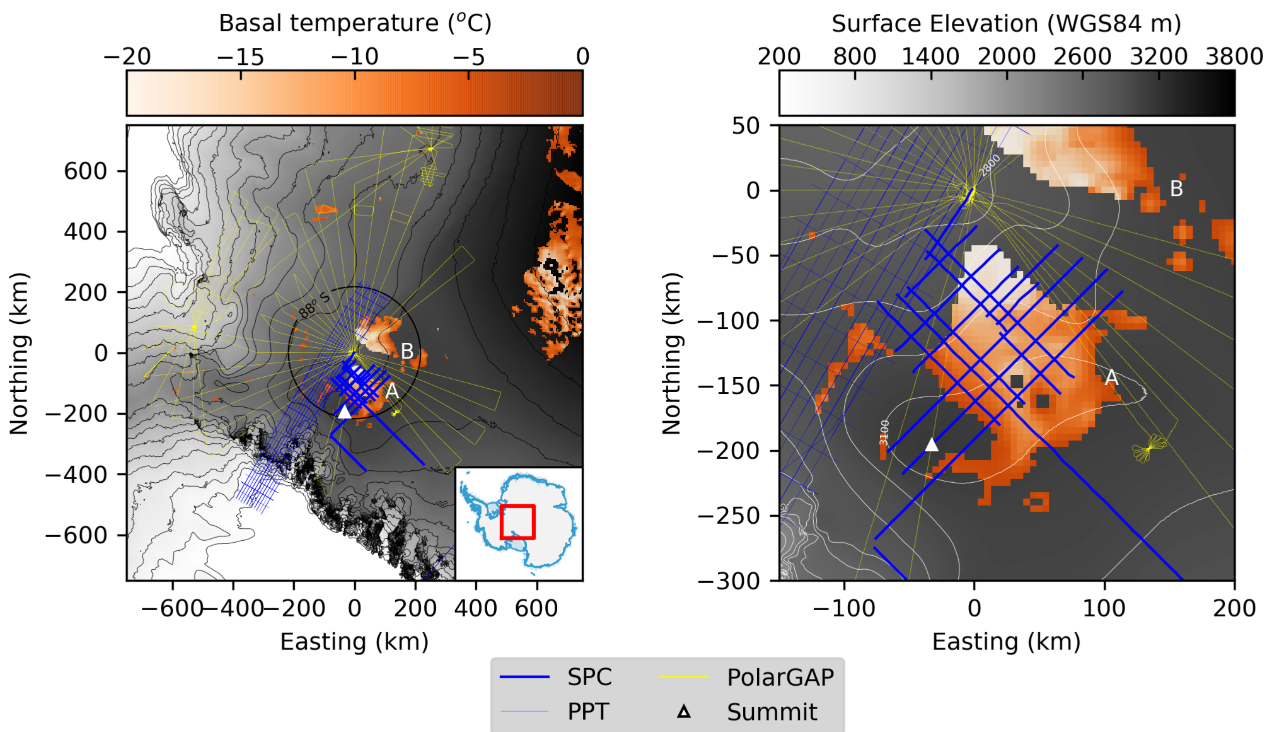

Figure 1. South Pole and Titan Dome region. ~~Flight~~ For both panels, flight lines from the South Pole Corridor (SPC) ~~, which is data presented here,~~ survey and previously published observations of Pensacola-Pole Transect ~~(PPT) from Carter et al. (2007)~~ (PPT; Carter et al., 2007) and PolarGAP (Jordan et al., 2018) surveys are also plotted. The orange shading are regions of increased paleoclimate ice core potential plotted as basal temperature (Van Liefferinge and Pattyn, 2013). The two ~~higher potential~~ coring candidate regions discussed in this paper are labeled ~~Candidate~~ A and B. The location of Titan Dome summit, as determined from the SPC survey, is the white triangle. The background shading and contours are from the Bamber et al. (2009) surface elevation DEM. The coordinate system used is polar stereographic (EPSG:3031).

helps propagate the age of internal reflecting horizons (IRH) throughout the region~~and add context to the new observations~~. The work presented here is part of an expanded mapping of IRH across the Antarctic Ice Sheet (e.g. Winter et al., 2019; Ashmore et al., 2020) .

In this paper, we describe new basal topography and surface elevation, identify areas on the flanks of Titan Dome that may have previously experienced faster flow than at present, and determine that the basal ice age is likely younger than would be needed to capture the middle Pleistocene transition.

2 Data

2.1 New Data

The SPC survey was conducted by an aero-geophysical suite installed on ~~a~~ the Polar Research Institute of China BT-67 airframe ~~(Cui et al., 2018) that contains~~ (Cui et al., 2018, 2020) that includes a coherent 60 MHz center frequency radar ice sounder (Peters et al., 2005), a laser altimeter, cesium magnetometer, three-axis stabilized gravimeter, and downward looking camera. The laser altimeter was a Riegl LD90-3800-HiP and collected data at 4 Hz, with an expected accuracy of 15 cm. Two survey flights were conducted, in February of ~~each~~ 2016 and 2017 (~~fig~~Fig. 1), over the area of Titan Dome~~that included coverage of a previously determined ice core target region (Van Liefferinge and Pattyn, 2013)~~. A grid ~~,~~ of roughly 150 km by 150 km with 25 km grid spacing ~~,~~ was surveyed. ~~A~~ One survey line was flown within 500 meters of the South Pole Ice Core ~~(Casey et al., 2014)~~ to enable the propagation of the core's ~~age model (Lilien et al., 2018)~~ chronology (Winski et al., 2019) throughout the region.

2.2 Existing Data

One older radar survey of the region is used in this analysis. The Pensacola-Pole Transect (PPT) was collected in ~~1998-1999. This~~ 1998–1999. These data was collected ~~on radar~~ with a radar system that was a direct ancestor of the system used for the ~~South Pole Corridor~~ SPC survey. The PPT survey used a 60 MHz center frequency with a 250 ns pulse width radar mounted on a Twin Otter airframe (Carter et al., 2007).

3 Methods

3.1 Radar Processing

The radar data was processed to a 1D focused state (Peters et al., 2007), without range migration. Focusing is applied to differentiate between nadir and off-nadir reflections and improve the resolution of the resulting radargram ~~. The processing increases~~ by increasing the discrimination of internal ~~structure within and beneath the~~ structures and the basal boundary of ice sheet.

The calculated basal reflection coefficient has been corrected for ~~energy loss due to the divergent beam pattern, also called~~ geometric spreading loss ~~,~~ and for assumed ice attenuation, which is primarily a function of ice temperature ~~(MacGregor et al., 2007)~~ (MacGregor et al., 2007; Matsuoka et al., 2012). Geometric spreading loss follows the standard theoretical relation using the infinite mirror approximation (e.g. Lindzey et al., 2020). ~~Dielectric attenuation is~~ This study uses an attenuation value of 10 dB km^{-1} everywhere and reported as two way travel ~~though~~ through a given ice thickness. ~~A value of 10 dB km^{-1} was used throughout the region. Although there is expectation that attenuation is~~ Although attenuation is expected to be variable due to spatial heterogeneity in ice temperature ~~profile~~ and/or ice chemistry, an attempt to constrain the variability is not made due to the numerous additional processes for which a control would be needed (e.g. subglacial water distribution, geothermal flux heterogeneity, ice chemistry, basal roughness). The relative consistency of low magnitude basal reflection and the lack of inferred basal water, as will be described later (section 4.2), support the assumptions used in determining the magnitude of the dielectric loss.

~~The attenuation valuewas determined by cross plotting basal reflectivity with ice thickness and regressing the distribution (fig~~To determine the attenuation value, multiple regressions (Fig. 2) ~~. Additional regressions that took a subset of the observations (thickness~~ with a combination of thickness distribution ($>$ 800 ~~, thickness~~ m and $>$ 1200 ~~) each resulted in attenuation of 7~~ m) and reflection values in each thickness bin (all, 5 highest, 5 lowest) resulted in a range of possible values (6–15 dB km^{-1}~~. To~~). Using the highest and lowest values in a bin attempts to isolate the effects of dialectic loss within the ice column ~~the highest or lowest values of reflectivity for a given ice thickness band can be used. In either case, the~~ by assuming the end member basal reflection coefficient is ~~assumed to be~~ consistent throughout the survey~~region and therefore isolates the effect of englacial attenuation. Specifically, the lowest and highest 5 values in each 50 m ice thickness bin were used. The number of values per bin has limited effect, changing the attenuation by only 2 dB km^{-1} when using 1 to 10 values in each thickness bin. Regression of the lowest values within each thickness bin (800 to 3000 m) results in an attenuation of 15 dB km^{-1}. The regression of the highest values results in 6 dB km^{-1}. As can be seen in fig. 2 the lowest value of reflectivity for the thinnest ice (500 to 1200 m) has a much steeper slope than the thicker ice. This could be due to the relative paucity of observations at these thicknesses. Ignoring the thinnest regions and regressing over 1200 to 3000 m of ice thickness and using the lowest values within each thickness bin results in attenuation of 11 dB km^{-1}. The same regression except with the highest values results in 9 dB km^{-1}. While some of these analysis choices are arbitrary the attenuation is likely between 7 and 15 dB km^{-1}. Theoretical values of attenuation for~~. A south polar ice column has an approximate average temperature of -35°~~C ice , the approximate average temperature of a south polar ice column (Beem et al., 2017) is within the range 7 and 15~~ C (Beem et al., 2017) and the theoretical values of attenuation for such ice is within 7–15 dB km^{-1}~~range~~, depending on ice chemistry (MacGregor et al., 2007). These values are also ~~consistent~~ in agreement with the results of an ice sheet wide estimate of englacial attenuation (Matsuoka et al., 2012)~~, which finds that the Titan Dome region has an attenuation consistent with the lower range of the estimates generated here~~. Consistent with theory and observations, 10 dB km^{-1} is used here.

3.2 Laser Altimetry Processing

Laser altimetry was corrected for biases in the attitude of the sensor ~~by~~ through minimization of the transect intersection differences (Young et al., 2015) with data from the ~~2015-2016~~ 2016 survey. As the laser and inertial navigation system was not removed from the aircraft between field seasons, recalibration of the second season was not required.

3.3 Surface, Bed, and Internal ~~Isochron~~ Reflecting Horizon Tracing

The manual ~~labeling~~ tracing of the surface and bed within the radar observations was consistent with the methodology described in Blankenship et al. (2001). The human ~~labelers~~ tracers applied a first return criteria to ~~label the horizons~~identify the bed. This has the effect of identifying the minimum possible ice thickness and smoothing basal topography, especially in regions with steep and variable relief. Using the traced ~~horizons~~ interfaces along with aircraft position the surface elevation, bed elevation, and ice thickness are determined. Radar wave speed in ice is ~~taken as~~ assumed to be 1.67x10^{8} m s^{-1}.

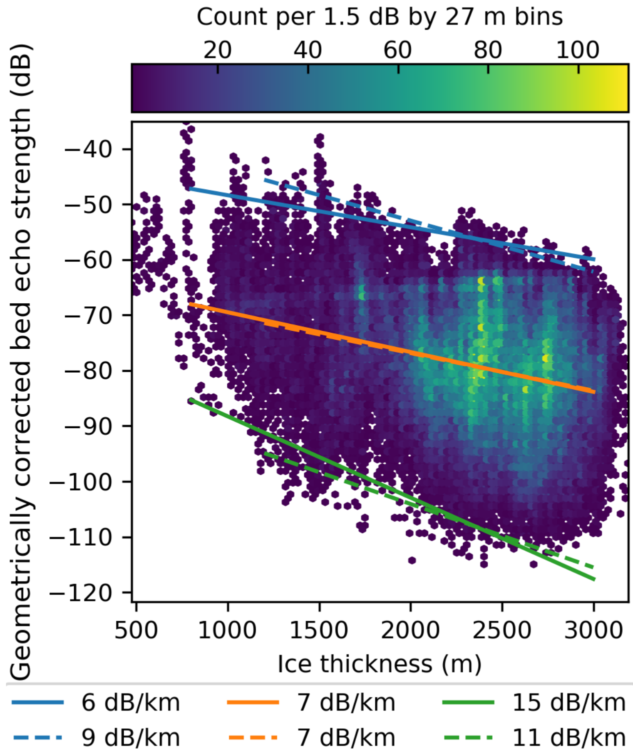

Figure 2. Attenuation determination. The color field represents the number of observations in each ~~27 m thickness bin and~~ 1.5 db geometrically-corrected echo strength by 27 m thickness bin. The solid lines are regressions using observations with ice thickness greater than ~~800m~~800 m, the dotted lines greater than ~~1200m~~1200 m. The orange lines use all observations in each thickness bin. The blue lines use the 5 highest echos strengths in each thickness bin and the green uses the 5 lowest. The legend reports the regression slope.

~~Isochrons~~ Internal reflecting horizons were manually traced using ~~industry software~~Landmark DecisionSpace semi-autonomous picking that uses the maximum value of the reflector. The South Pole Ice Core ~~age model (Casey et al., 2014)~~ chronology (Winski et al., 2019) was projected onto the radargram that flew most proximal to the core location (∼500 m), by correlating the ice depth of both the ice core and radar observations. Where ~~isochrons are contiguous~~ IRH are completely continuous the age record ~~can be propagatedthroughout the surveyed region. Nine age isochrons were propagated~~ was propagated. Internal reflecting horizons may have discontinuities in visibility due to dip steepness, being obscured by radar clutter, the effects or radar processing, or ceasing to generate a suitably strong reflection for other reasons (Siegert, 1999; Harrison, 1973; Holschuh et al., 2014) . Nine dated IRH were traced to their maximum possible extent from the South Pole Ice Core: 0 ka (taken as the surface), 4.7 ka, 10.7 ka, 16.8 ka, 29.1 ka, 37.6 ka, 51.4 ka, 72.5 ka, and 93.9 ka.

The surface, bed, and ice thickness were compared to widely used community data sets (Fretwell et al., 2013; Bamber et al., 2009; Helm by interpolating the gridded data to each geophysical observation location using a bivariate spline approximation.

3.4 Basal Ice Age Model

The age of the basal ice (a) can be modeled with the constraints ~~from the dated isochrons~~provided by radar observations and dated IRH. Two 1D models are compared to estimate the age of the basal ice. One model uses the simplest Nye assumptions which are a steady state ice thickness (H) and a constant strain rate with depth ~~(Cuffey and Paterson, 2010, eq. 15.8).~~ (Cuffey and Paterson, 2010, Eq. 15.8),

$$a = \frac{H}{b} ln\left(\frac{1}{1 - z/H}\right). \tag{1}$$

For this model, ~~vertical strain is only dependent on~~ there is only one unknown parameter, surface accumulation rate (b), and basal ice is arbitrary defined as a depth (z) 30 meters above the bed. Ice thickness (H) is defined by radar observations. The model is ~~solved~~ run for each vertical ~~record independently by finding~~ radar observation independently by solving for the accumulation rate that minimizes the root mean squared error between the age model and the traced ~~isochrons~~IRH. The resulting accumulation field enables an estimate of the spatial patterns of average accumulation rate. Comparing the spatial distribution of accumulation from the model to ~~observations of accumulation (Arthern et al., 2006; Wessem et al., 2014)~~ independent observations/modeling of accumulation (Arthern et al., 2006; Wessem et al., 2014; Studinger et al., 2020) serves as partial ~~verification of the model~~ model verification.

The second age model ~~makes~~ uses the Dansgaard-Johnson set of assumptions concerning vertical strain rates ~~(Cuffey and Paterson, 2010, . In addition to setting an accumulation rate for the model, a characteristic height~~ (Cuffey and Paterson, 2010, Eq. 15.14 and 15.15)

,

$$a = a' + \frac{2H - h}{b} + \left(\frac{h}{z} - 1\right) \tag{2}$$

$$a' = \frac{2H - h}{2b} ln\left(\frac{2H - h}{h}\right). \tag{3}$$

A characteristic height (h) above the bed ~~is set to mark~~ marks the transition from constant vertical strain above to linearly varying to zero below. A range of transitional heights ~~are tested, 0.2 to 0.5 of the~~ (h) were tested, 20% to 50% of ice thickness above the bed. In this model, z is height above bed. The Dansgaard-Johnson model is solved independently for each vertical radar observation by solving for the accumulation (b) that minimizes the root mean squared misfit between the model age and the dated IRH. This model is highly sensitive to accumulation rate, which ~~sets~~ determines the magnitude of vertical strain, but less sensitive to the chosen transitional height. Additionally, the model is sensitive to the definition of basal ice~~has a sensitive effect on the determined basal ice age~~, given the high degree of non-linearity this model produces ~~in the deepest ice~~near the bed. To improve on the arbitrarily defined 30 m above the bed, a minimum desired temporal resolution of ice, 10 kyr m^{-1} (Fischer et al., 2013), is used to determine the basal ice age. The ~~age when~~ basal age output of the model is the age at the depth where this temporal resolution threshold is exceeded~~is considered the basal ice age. The Dansgaard-Johnson model is solved independently for each vertical record by finding the accumulation that minimizes the model age and dated isochron root mean squared error misfit.~~ .

3.5 Submergence

Investigating the submergence rate, the ~~length per unit time~~ speed that a dated ~~isochron~~ IRH takes to reach its current position, can be informative of the flow history in the region. Submergence rate is calculated ~~in the same manner as Beem et al. (2017) . We use the linear variability of strain rates,~~ with published methodology (Beem et al., 2017) and assuming m=1~~in eq 6 of Beem et al. (2017). Basically, the~~ ,

$$w = -b\left(\frac{z}{H}\right)^{m}. \tag{4}$$

The model assumes the form of the vertical strain rate profile and determines the magnitude of vertical strain necessary to submerge an ~~isochron~~ IRH of a given age to its observed depth. Submergence rates (w) are calculated for each dated ~~isochron-bounded-interval~~ IRH-bounded-interval within the ice column. In the above equation, b is ice equivalent surface accumulation, H is ice thickness, and z is height above the bed. There is a correction step that removes the influence of the strain from each younger interval ~~. Spatial patterns~~ (Beem et al., 2017). Patterns in submergence that exceed expected spatial gradients in accumulation are interpreted to represent ~~spatial~~ heterogenous basal melt or ice flow. The results create a temporal history that ~~is significant for interpreting the timing of any changes in~~ can be interpreted as changes to processes that effect submergence rates (e.g. accumulation, basal melt, and/or horizontal strain).

4 Results

4.1 Bed ~~and~~ Topography, Surface Elevation, and Ice Thickness~~The bed and surface elevation observed~~

The bed elevation determined by radar reflection ~~constrain the location of the ice topographical high of the dome and~~ reveal a mountainous subglacial terrain that was previously unknown. The bed ~~topography includes multiple bedforms with over 1000 m of prominence (fig~~is rugged, with >1 km of relief along the survey lines and bed slopes of up to 45° (Fig. 3 and 7). The 20 km line spacing does not resolve the extent of these features, and the effectiveness of mass conservation methods of bed interpolation is limited by low ice velocities (Morlighem et al., 2020), restricting the use of only 1-D modeling approaches. The new observations suggest that the main ice dome is located on a basal topographic high instead of a valley. The ice thickness in this region is therefore commensurately thinner than previously estimated (Fretwell et al., 2013).

There are two independent surface elevation DEMs of the Titan Dome region (Bamber et al., 2009; Helm et al., 2014) ~~. Other~~ which other gridded DEM products (e.g. Bedmap2, REMA, BedMachine) use ~~one of these two~~ to fill in ~~the~~ their data gaps south of 86° South (Fretwell et al., 2013; Howat et al., 2019; Morlighem et al., 2020)~~, but can deviate from the source~~

~~data due to the specific gridding and mosaicking implementation~~. Generally, there is good agreement between the available DEM products and the new ~~laster~~ laser altimetry observations of surface elevation (~~fig.~~ Fig. 3 and 4). The Bamber et al. (2009) DEM is 20 +/- 62 m (average +/- 2 standard deviations) higher than the SPC radar observations and the Helm et al. (2014) DEM is 23 +/- 73 m higher. The Titan Dome summit location differs by at least 34 km between the Bamber et al. (2009) and Helm et al. (2014) DEMs~~by at least 34 km. The aerial surface altimetry , collected here ,~~. The surface altimetry collected here is sparse and cannot explicitly constrain the location of the Titan Dome, but the dome location in ~~the Bamber et al. (2009)~~ Bamber et al. (2009) DEM was used in survey planning and ~~is~~ corresponds to the location of highest elevation observed in this survey. The dome elevation is observed to be 3154 m and occurs at -88.1716° N, ~~-99.5234~~-170.4765° E~~, which~~. This location is within 10 m ~~of the Bamber et al. (2009) elevation and corresponds with their location of maximum surface elevation.~~ elevation and at the same position as the Bamber et al. (2009) defined summit.

The bed elevation and ice thickness of the SPC survey compared to the Bedmap2 dataset shows significant variance. Bedmap2 is 30 +/- 550 m (average +/- 2 standard deviations) thicker than the SPC radar observations. 50% of the radar observations within candidate A (Fig. 1) have thinner ice than Bedmap2 when interpolated from the grid. Given the gridded nature, 69% of the Bedmap2 pixels within candidate A that were surveyed have thicker ice than the radar observations. The region of the SPC survey only had sparse observations previously available and differences between the available gridded datasets and the new observations are expected.

4.2 Basal Reflectivity

The bed beneath Titan Dome and the surrounding region show generally low reflectivity and heterogenous character. ~~Isolated~~ Localized regions of higher values (> -30 db) are observed in the subglacial drainages that ~~flows~~ flow towards the Filchner-Ronne Ice Shelf ~~and corresponds to basal topographic troughs (blue polygon in fig. 5~~(generally grid north or northwest). Higher values are also seen ~~above the summit of the newly described subglacial mountain (blue circle in fig. 5) and an isolated location near the end of a survey line (green diamond in fig. 5 near 100 km ,~~beneath a region of thin ice (Fig. 5 near 0 km easting and -50 km ~~PS71 coordinates~~northing).

The ~~distribution~~ low values of basal reflectivity suggests that the basal ice beneath ~~the dome~~ Titan Dome region is frozen to the bed ~~with~~ and there is limited basal melt and water movement. This conclusion is consistent with previous basal temperature modeling efforts ~~(e.g. Beem et al., 2017; Van Liefferinge and Pattyn, 2013; Price et al., 2002)~~ (e.g. Beem et al., 2017; Van Liefferinge et al that conclude the bed in the region is 10° C or more below the pressure melting temperature. ~~The exception may be in the main drainage from the dome towards the Filchner-Ronne Ice Shelf which shows higher reflectivity magnitudes, including some of the highest values observed in this survey (blue polygon in fig. 5).~~ It is unlikely that ~~pools~~ bodies of water were ~~sampled~~detected by radar, but the ~~reflectivity~~ local reflectivity maximums suggests a higher likelihood of a smoother bed and/or small amounts of basal water in ~~this region~~these regions, potentially in the form of saturated sediments or interfacial water. The high reflectivity ~~is seen near the summit of the subglacial high~~ seen beneath shallow ice may be the result of the ~~shallow ice conditions of this location and attenuation correction~~ attenuation correction that is too large for the ~~thin~~ cold ice expected ~~above this region~~there.

4.3 Basal Ice Age

~~Two age~~

Two models were used to estimate the age of the basal ice, ~~using the dated isochron as constraints~~each constrained by radar observations and dated IRH. The Nye age model ~~, predict~~ calculates basal ages as old as ~~350 kawith~~ 360 ka, but much of the region is younger. The modeled accumulation field used to minimize the misfit between dated IRH and modeled ages have a mean accumulation (in ice equivalent) of 4.4 cm yr^{-1}. The spatial distribution of accumulation ~~rates show lower magnitudes on the highest surface elevation of the dome~~ has lower magnitudes near the dome summit (3 to 5 cm/yr) and higher rates at lower elevations (up to 9 cm/yr). This pattern and ~~magnitudes are~~ magnitude is generally consistent with space-borne and re-analysis estimates of accumulation patterns of the region (Arthern et al., 2006; Wessem et al., 2014). ~~This~~ The highest values of accumulation are seen in a region of a broad flat ice surface topographic trough. This matches a recent accumulation study (Studinger et al., 2020) that finds 3 to 5 cm/yr accumulation on the summit and implies higher values of accumulation, up to 20 cm/yr, in the ice surface trough due, in part, to katabatibc wind steering. This age model result is not expected to be predictive of modern accumulation rates, and there are ~~regions that show higher magnitude than~~ deviations from available observations, however the general patterns are plausibly realistic and lend credence to the model performance despite its simplicity.

The Dansgaard-Johnson age model calculates older ages ~~due to the model assumptions that include~~ than the Nye model due to assumptions that lead to smaller magnitude vertical strain rates near the bed. Isolated regions exceeding 1 Ma of age are predicted to exist in the most favorable parameter sets, however ages between 600 and 800 ka are more typical. The higher the transitional height in the Dansgaard-Johnson model the older the maximum basal age due to a greater proportion of the ice thickness with smaller vertical strain rates. With a transitional ~~depth of 0.2~~ height (h) at 20% of ice thickness the maximum age was ∼0.9 Ma and when the ~~transition depth is 0.5~~ height is at 50% of ice thickness the maximum age ~~increases~~ increased to greater than 1.4 Ma. In every model case the probability of suitably old ice to capture the middle Pleistocene transition is low.

The height above the bed of basal ice used by the Dansgaard-Johnson model ranges from 5 to 120 meters, due to defining it with a temporal threshold of the model output. When the transitional height (h) is 20% of ice thickness the mean basal ice is 61 m above the bed and when h is 50% the mean basal ice is 79 m above the bed. Spatial variability in accumulation patterns and magnitudes were consistent with the Nye model results, with less accumulation on the dome (∼2 cm yr^{-1}) and higher amounts on the flanks (up to 10 cm yr^{-1}). ~~In every model case the probably of suitably old ice to capture of the middle Pleistocene transition is low. Age model results. The top row are the results of the Nye model assumptions and the bottom row the results of the Dansgaard-Johnson set of assumptions. The RMSE fit is the difference between the model and the traced and dated internal isochrons. Each panel is plotted over the higher probability candidate A ice core target region in orange (Van Liefferinge and Pattyn, 2013) and 100 m surface elevation contours (Helm et al., 2014). The dome is surrounded by the 3100 m contour.~~

At an ice divide, the Dansgaard-Johnson model ~~is best~~ may best be applied with a transitional height that equals ice thickness, ~~the strain rate~~ resulting in a vertical strain rate that varies linearly from the surface to the bed (Cuffey and Paterson, 2010, p. 619). In this scenario, the basal ages become considerably older, at multiple millions of years. Although ~~,~~ such a strain rate profile is only relevant for a small portion of the survey, it creates a hypothetical that if the dome position was highly stable, the local conditions would create a suitable site for the extraction of an ice core that captures the middle Pleistocene transition. However, dome stability over these timescales is generally not expected, particularly for Titan Dome given its proximity to ~~major and~~ dynamic ice drainages (Trans-Antarctic mountain outlet glaciers and Filchner-Ronne ice streams) and ~~the~~ evidence that suggest the region has experienced more rapid flow in the past ~~(Section 4.4)~~(Section 4.4; Beem et al., 2017; Lilien et al., 2018; Bingham et al., 2007 .

4.4 ~~Dated Isochron~~ Internal Reflecting Horizon Depth and Submergence

~~Nine dated isochrons~~

Nine dated IRH were traced to their maximum extent. The younger ~~isochrons~~ IRH were traceable throughout the entire survey region, but older ~~isochrons~~ IRH suffered from discontinuities ~~and were increasingly limited in the extent in which they could be traced. Isochrons may have gaps in visibility due to dip steepness, being obscured by radar clutter, or ceasing to generate a suitably strong reflection for other reasons. The limited intersections of survey lines impede tracingaround areas without isochron visibility~~that prevented tracing. The 72.5 ka ~~isochron~~ IRH was traced throughout a majority of the survey, but it was not possible to trace the 93.9 ka ~~isochron~~ IRH beyond a few 10s of km from the ice core location.

The fractional depth of the 72.5 ka ~~isochron~~ IRH ranges from 43% to 78% of the ice depth with a mean of 60% (~~fig. 6 and 7~~ Fig. 7 and 8). The ~~southern side of the dome~~ surveyed dome flanks show the deepest fractional depth for any given ~~age isochron, as do regions near the prominent bedrock features (fig. 7). The observed depth of the 72.5 ka isochron significantly reduces the likelihood of sufficient temporal resolution if ice greater than 1 Ma old were to exist within the survey~~IRH. Shallower IRH depths exist nearer the present day ice divide between Titan Dome and South Pole.

~~The~~ Present day flow over Candidate A is less than 2 m yr^{-1}, however submergence calculations put bounds on the timing of ~~past ice flow deceleration~~faster ice flow in the past. For the interval starting ~~with~~ at the present, 0 to 4.7 ka, the ~~gradients (fig~~submergence gradients (Fig. 8b) ~~of submergence a~~ are similar to both the magnitude and pattern of present day accumulation ~~(Arthern et al., 2006; Wessem et al., 2014)~~(Arthern et al., 2006; Wessem et al., 2014; Studinger et al., 2020), suggesting that this interval has been dominated by accumulation driven vertical strain. Similar to the conclusions of Beem et al. (2017), the submergence rates from the interval 10.7 to 16.8 ka (~~fig~~Fig. 8c) show strong, but transitional, submergence boundaries. The ~~10.7 to 16.8 interval is the transition between the~~ 4.7 to 10.7 ka submergence (not pictured) ~~which~~ is very similar to the 0 to 4.7 ka interval, and the 16.8 to 29.1 ~~(fig~~ka interval (Fig. 8d) ~~which also~~ shows high gradient boundaries in submergence. This suggests ~~the regional higher magnitude~~ a region of greater vertical strain ceased during the 10.7 to 16.8 ka interval. The new SPC observations show a contiguous region of greater submergence ~~,~~ that is isolated to a single ice catchment~~, that is bounded by higher gradients of submergence~~ . Together this supports the notion that the submergence is caused by ice dynamic processes. Regional geothermal flux anomalies cannot explicitly be excluded. But, the region of elevated submergence is bounded by high submergence gradients that are difficult to ascribe solely to accumulation patterns or geothermal flux, suggesting the hypothesis that ice dynamics are driving higher submergence rates.

~~Example radargrams with traced isochrons. A context map is in the upper left corner. Beneath each panel is the bed echo strength, which when it exceeds -30 db is highlighted with vertical green lines, the same regions highlighted in fig. 5. The white vertical line on each radargram represents the crossover of the two transects.~~

5 Discussion

Titan Dome has been previously identified ~~(Van Liefferinge and Pattyn, 2013)~~ (Van Liefferinge and Pattyn, 2013; Van Liefferinge et al., 20 as a region that holds potential for an ice core that would capture the middle Pleistocene transition (1.25 Ma to 0.7 Ma), due to slow flow, appropriate ice thickness, and the likelihood of basal temperatures that are well below the pressure melting point ~~(Van Liefferinge and Pattyn, 2013; Beem et al., 2017; Price et al., 2002)~~(Van Liefferinge and Pattyn, 2013; Van Liefferinge et al., 2018; B . The analysis completed here shows that the basal ice age is likely too young to be relevant for examination of the middle Pleistocene transition. While ~~Titan Dome~~ much of the Titan Dome region has ice of appropriate thickness, the dated ~~isochron~~ IRH of 72.5 ka ~~are~~ is at a significant fractional depth (~~50 to 70%), deceasing~~ 0.5 to 0.7), decreasing the likelihood of suitably old ice and severely limiting the temporal resolution of old ice if it were to exist (~~fig~~Fig. 8a). In comparison, Little Dome C of East Antarctica, has a 72 ka ~~isochron~~ IRH modeled to be between ~~25% and 30%~~ 0.25 and 0.3 of the ice depth (Parrenin et al., 2017).

The ~~basal ice age~~ models for Titan Dome fail to calculate ice of suitably old age. The Dansgaard-Johnson model, with assumptions that produce highly non-linear ~~age~~ ages approaching the bed, finds only isolated regions of 1.4 Ma in basal ice age. Although it is encouraging that the oldest modeled ages are on the dome and flanking ice divides, a typically suitable location for drilling an ice core (Van Liefferinge and Pattyn, 2013; Fischer et al., 2013; Van Liefferinge et al., 2018; Passalacqua et al., 2018) , the specific locations with the oldest ages in this study have been previously excluded from consideration due to exceeding the modern ice flow threshold of 2 m yr^{-1} (Van Liefferinge and Pattyn, 2013).

The ~~ice sheet modeling that identifies cold bedded drilling regions at Titan Dome (Van Liefferinge and Pattyn, 2013) used Bedmap2, which reports generally thicker ice than the SPC radar observations , Bedmap2 is 30 +/- 550 m (average +/- 2 standard deviations) thicker than the SPC radar observations. 50% of the radar observations within candidate A have thinner ice than Bedmap2 when linearly interpolated from the grid. Given the gridded nature of~~ new observations have the ~~modeling, 69% of the Bedmap2 pixels within the promising area that were surveyed have thicker ice than the radar observations~~effect of reducing the area of suitable regions identified by ice sheet modeling (Van Liefferinge and Pattyn, 2013). The effect of ~~thinner ice on the Van Liefferinge and Pattyn (2013) modeling~~ the observed thinner ice, compared to Bedmap2 used to identify candidate A, is two fold and would have competing effects. Thinner ice would tend to increase the ~~size of the promising region~~ area of the region suitable for recovering middle Pleistocene age ice, because fewer locations would exceed their geothermal heat flux threshold for melting. Thinner ice would~~also decrease the extent of the promising region by increasing the balance velocities used to eliminate regions with excessive horizontal ice~~ , however, increase calculated balance velocities excluding more area due to excessive horizontal advection. The ~~Titan Dome region~~ Candidate A boundary is more ice flow limited than temperature limited and the net effect of thinner ice would likely be a reduction in the extent of the promising region. For instance, the area between candidates A and B is excluded from Van Liefferinge and Pattyn (2013) because it exceeds ~~the~~ their balance velocity threshold ~~(~~of $>$2 m yr^{-1}~~). Additionally, some areas would be excluded as they are not thicker than the 2000 m threshold~~, also see Bingham et al. (2007).

~~Titan Dome also shows~~ The flanks of Titan Dome show evidence of increased ice flow in the past, ceasing between 10.7 and 16.8 ka. This flow history could result in the loss of basal ice through basal melting and complications in stratigraphic layering due to elevated strain rates. Recent publications have indicated past ice flow on the flanks of Titan Dome ~~that~~ is consistent with ice stream transitional flow (Beem et al., 2017; Lilien et al., 2018), that between slow ice deformation dominated flow in the interior ice sheet and ~~that of~~ basal slip dominated ice streaming. ~~Isochron drawdown in the region~~ Given this dynamic history the dome may be prone to divide migration (Winter et al., 2018). Internal reflecting horizon drawdown is consistent with ~~local~~ one or more of the following: regional melt from elevated geothermal flux, extensional strain ~~, and/or~~ from ice flow, and frictional heating from past ice dynamics. The ~~drawn down pattern , clearly evident in fig~~drawdown pattern includes a linear boundary (see arrow in Fig. 8(a)~~, includes a linear boundary that passes through PS71 50 km easting and 50 km northing and~~) and is completely within a single ice catchment, which supports an ice dynamically induced drawdown. The linear boundary has previously been interpreted is a relic shear margin (Beem et al., 2017). The ~~drawn down~~ IRH drawdown (expressed both as elevated submergence and greater IRH depth) seen in the new SPC observations are consistent and contiguous with the pattern from the older ~~Pensicola-Pole Transects observations.~~

~~Previous work (Beem et al., 2017) has suggested that the region decelerated between 10.7 and 16.8 ka. The submergence calculations from the SPC observations regions support the same conclusion that for a period ending between 10.7 and 16.8 ka the region experienced flow sufficient enough for vertical strain to be driven by horizontal ice flow gradients, such as from ice streaming or transitional flow. The ice streaming processes evident in drawdown of isochrons make the~~ PPT observations. The evident ice streaming processes makes this region more complicated for paleoclimate age model construction and the survivability of ice greater than 1 Ma.

~~The distribution of maximum basal echo strength locations is consistent with the regions of increased submergence, suggesting that this region may have experienced greater basal heating in the past. A hypothesis put forth in Beem et al. (2017) suggests that remanent heat from past sliding may contribute to the present distribution of basal reflectivity and subglacial water. This hypothesis is generally supported by the new observations which show a contiguous region of increased submergence that is also has higher average basal reflectivity than the surrounding region. If this observation is representative of ice sheet dynamics, at least portions of the promising ice core target experienced faster flow in the past, which would decrease or eliminate its suitability for extracting an interpretable climate record, especially for one that extends to 1 Ma or beyond.~~

Candidate B (~~fig~~Fig. 1), a region of modeled cold based ice, ~~north along~~ along the ~45°E meridian from South Pole, does not show enhanced flow history expressed through submergence rates (Beem et al., 2017). Using the same dated ~~isochrons~~IRH, but traced wholly within the older ~~Pensicola-Pole Transects~~ PPT data (Carter et al., 2007), the thickness of ice below the 93.9 ka ~~isochron~~ IRH is generally less than ~~1000 m~~1200 m, and in some ~~instances lessthan 750 m.~~ cases considerably less. The percent depth for the 93.9 ka IRH is 60 to 70%. At least for the region with radar observations~~, it is unlikely that any ice~~ . If any ice were greater than 1 Ma~~would~~ , It is unlikely to have suitable temporal resolution.

The role or existence of elevated geothermal heat flux in the study region is difficult to determine, but there is limited evidence to support its existence. Previous work has suggested a region proximal to Titan Dome has elevated geothermal flux (Jordan et al., 2018)~~. However,~~ , but the basal characterization of Titan Dome neither confirms ~~or~~ nor refutes the existence of elevated geothermal flux outside of the SPC survey area. The new survey presented here is of a different subglacial catchment than that ~~described in~~ identified to host elevated geothermal flux by Jordan et al. (2018) and heterogeneity in geothermal flux is expected over length scales of 100s of kilometers. The basal ~~characterization~~ reflectivity of Titan Dome does show a few localized areas with a higher likelihood for the existence of water. It is possible that localized geothermal flux could be causing the increased basal reflectivity, which may be in addition to or an alternative hypothesis to remnant heat from past basal sliding (Beem et al., 2017). These hypotheses could be tested through direct access of the bed to characterize the geology and measure geothermal flux.

6 Conclusions

Titan Dome is unlikely to be a suitable site for the extraction of ~~ice for a climate proxy~~ an ice core that captures the middle Pleistocene transition. The ~~dated isochrons~~depth of dated IRH, the age models, and implications for faster flow ~~in the past~~ that ceased during the last glacial maximum are each discouraging to the possibility of suitably old ice. Age models all indicate ~~the~~ basal ice age between 300 and 800 ka in the most promising locations. Older modeled ages do occur in some regions when using ~~more favorable~~ end member model parameters. In all instances, ~~this~~ the age is younger than the ~~1.25~~ 1.5 Ma ice needed to study the complete middle Pleistocene transition. If 1 Ma or older ice were to exist, ~~isochron ages ,~~ IRH ages that are dated and propagated from the South Pole Ice Core ~~(Casey et al., 2014)~~(Casey et al., 2014; Winski et al., 2019), are too deep to have a suitable ~~amount of ice for high~~ temporal resolution. Further complication to any extracted ice core from Titan Dome is the evidence for faster flow in the past, which would distort chronology and source regions for any given layer within the core.

The new observations also ~~described~~ describe previously unknown basal topography ~~, including a large subglacial mountain. The new observations~~ that can be used to further improve community data sets in this region, they ~~are already within~~ have already been added to the BedMachine product (Morlighem et al., 2020). The location of the Titan Dome summit is observed to be consistent with the Bamber et al. (2009) ice surface DEM and located at -88.1716° N, ~~-99.5234~~ -170.4765° E.

Data availability. The L2 data is made available at USAP data portal [URL to be provided]

Author contributions. This project was made possible by funding acquired by DDB, DAY, JG and SB and project administration by DAY, DDB, JG, SB. Conceptualization of the project was completed by LHB, DAY, MPGC, and JSG with investigation by JSG. Formal analysis and visualization was completed by LHB. Methodology was developed by LHB and MGCP. LHB wrote the original draft and all authors contributed to review and editing. Data curation was completed by DAY and LHB.

Competing interests. The authors declare they have no conflict of interest.

Acknowledgements. The authors would like to thank Polar Research Institute of China for their support and making their aerial geophysical platform available for this research. The authors also thank Ken Borek Ltd. pilots and engineers for ~~the~~ their involvement and support in data collection. The authors thank Mercy Grace Browder and Roccio Castillo for their efforts in radar interpretation and the support of the Jackson School for Geoscience GEOFORCE program. The work here was supported by NSF Grant #1443690 (SPICECAP), G. Unger Vettlesen Foundation, the National Natural Science Foundation of China (41876227) and the National Key R&D Program of China (2018YFB1307504). We thank Massimo Frezzotti and Neil Ross for their thoughtful and helpful reviews. This is UTIG contribution #XXXX.

References

An, M., Wiens, D. A., Zhao, Y., Feng, M., Nyblade, A., Kanao, M., Li, Y., Maggi, A., and Lévêque, J.-J.: Temperature, lithosphere-asthenosphere boundary, and heat flux beneath the Antarctic Plate inferred from seismic velocities, Journal of Geophysical Research: Solid Earth, 120, 8720–8742, https://doi.org/10.1002/2015JB011917, 2015.

Arthern, R. J., Winebrenner, D. P., and Vaughan, D. G.: Antarctic snow accumulation mapped using polarization of 4.3-cm wavelength microwave emission, Journal of Geophysical Research: Atmospheres, 111, D06 107, https://doi.org/10.1029/2004JD005667, 2006.

Ashmore, D. W., Bingham, R. G., Ross, N., Siegert, M. J., Jordan, T. A., and Mair, D. W.: Englacial architecture and age-depth constraints across the West Antarctic Ice Sheet, Geophysical Research Letters, 47, e2019GL086 663, https://doi.org/10.1029/2019GL086663, 2020.

Augustin, L., Barbante, C., Barnes, P. R., Barnola, J. M., Bigler, M., Castellano, E., Cattani, O., Chappellaz, J., Dahl-Jensen, D., Delmonte, B., et al.: Eight glacial cycles from an Antarctic ice core, Nature, 429, 623–628, https://doi.org/10.1038/nature02599, 2004.

Bamber, J., Gomez-Dans, J., and Griggs, J.: A new 1 km digital elevation model of the Antarctic derived from combined satellite radar and laser data–Part 1: Data and methods, The Cryosphere, 3, 101–111, https://doi.org/10.5194/tc-3-101-2009, 2009.

Beem, L. H., Cavitte, M. G. P., Blankenship, D. D., Carter, S. P., Young, D. A., Moldoon, G., Jackson, C. S., and Siegert, M. J.: Ice-flow reorganization within the East Antarctic Ice Sheet deep interior, in: Exploration of Subsurface Antarctica: Uncovering Past Changes and Modern Processes, edited by Siegert, M. J. and Jamieson, S. R. abd White, D. A., vol. 461, Geological Society of London, https://doi.org/10.1144/SP461.14, 2017.

Bingham, R. G., Siegert, M. J., Young, D. A., and Blankenship, D. D.: Organized flow from the South Pole to the Filchner-Ronne ice shelf: An assessment of balance velocities in interior East Antarctica using radio echo sounding data, Journal of Geophysical Research: Earth Surface, 112, F03S26, https://doi.org/10.1029/2006JF000556, 2007.

Blankenship, D., Morse, D., Finn, C., Bell, R., Peters, M., Kempf, S., Hodge, S., Studinger, M., Behrendt, J. C., and Brozena, J.: Geologic controls on the initiation of rapid basal motion for West Antarctic ice streams: A geophysical perspective including new airborne radar sounding and laser altimetry results, The West Antarctic ice sheet: behavior and environment, 77, 105–121, https://doi.org/10.1029/AR077p0105, 2001.

Carter, S. P., Blankenship, D. D., Peters, M. E., Young, D. A., Holt, J. W., and Morse, D. L.: Radar-based subglacial lake classification in Antarctica, Geochemistry Geophysics Geosystems, 8, Q03 016, https://doi.org/10.1029/2006GC001408, 2007.

Casey, K. A., Fudge, T. J., Neumann, T., Steig, E. J., Cavitte, M., and Blankenship, D. D.: The 1500 m South Pole ice core: recovering a 40 ka environmental record, Annals of Glaciology, 55, 137–146, https://doi.org/10.3189/2014AoG68A016, 2014.

Clark, P. U., Archer, D., Pollard, D., Blum, J. D., Rial, J. A., Brovkin, V., Mix, A. C., Pisias, N. G., and Roy, M.: The middle Pleistocene transition: characteristics, mechanisms, and implications for long-term changes in atmospheric pCO2, Quaternary Science Reviews, 25, 3150–3184, https://doi.org/10.1016/j.quascirev.2006.07.008, 2006.

Cuffey, K. M. and Paterson, W. S. B.: The Physics of Glaciers, Butterworth-Heinemann, fourth edn., 2010.

Cui, X., Greenbaum, J. S., Beem, L. H., Guo, J., Ng, G., Li, L., Blankenship, D., and Sun, B.: The First Fixed-wing Aircraft for Chinese Antarctic Expeditions: Airframe, modifications, Scientific Instrumentation and Applications, Journal of Environmental and Engineering Geophysics, 23, 1–13, https://doi.org/10.2113/JEEG23.1.1, 2018.

Cui, X., Greenbaum, J. S., Lang, S., Zhao, X., Li, L., Guo, J., and Sun, B.: The Scientific Operations of Snow Eagle 601 in Antarctica in the Past Five Austral Seasons, Remote Sensing, 12, 2994, https://doi.org/10.3390/rs12182994, 2020.

Fischer, H., Severinghaus, J., Brook, E., Wolff, E., Albert, M., Alemany, O., Arthern, R., Bentley, C., Blankenship, D., Chappellaz, J., and et al.: Where to find 1.5 million yr old ice for the IPICS "Oldest-Ice" ice core, Climate of the Past, 9, 2489–2505, https://doi.org/10.5194/cp-9-2489-2013, 2013.

Fretwell, P., Pritchard, H. D., Vaughan, D. G., Bamber, J. L., Barrand, N. E., Bell, R. E., Bianchi, C., Bingham, R. G., Blankenship, D. D., Casassa, G., Conway, H. B., Cook, A. J., Corr, H. F. J., Damaske, D., Damm, V., Ferraccioli, F., Forsberg, R., Fujita, S., Gim, Y., Gogineni, S., Griggs, J. A., Hindmarsh, R. C. A., Holmlund, P., Holt, J. W., Jacobel, R. W., Jenkins, A., Jokat, W., Jordan, T., King, E. C., Kohler, J., Krabill, W. B., Riger-Kusk, M., Langley, K. A., Leitchenkov, G., Leuschen, C., Luyendyk, B. P., Matsuoka, K., Mouginot, J., Nitsche, F. O., Nogi, Y., Nost, O. A., Popov, S. V., Rignot, E. J., Rippin, D. M., Rivera, A., Roberts, J., Ross, N., Siegert, M. J., Smith, A. M., Steinhage, D., Studinger, M., Sun, B., Tinto, B. K., Welch, B. C., Wilson, D., Young, D. A., Xiangbin, C., and Zirizzotti, A.: Bedmap2: improved ice bed, surface and thickness datasets for Antarctica, The Cryosphere, 7, 375–393, https://doi.org/10.5194/tc-7-375-2013, 2013.

Gooch, B. T., Young, D. A., and Blankenship, D. D.: Potential groundwater and heterogeneous heat source contributions to ice sheet dynamics in critical submarine basins of East Antarctica, Geochemistry, Geophysics, Geosystems, 17, 395–409, https://doi.org/10.1002/2015GC006117, 2016.

Harrison, C. H.: Radio echo sounding of horizontal layers in ice, Journal of Glaciology, 12, 383–397, https://doi.org/10.3189/S0022143000031804, 1973.

Helm, V., Humbert, A., and Miller, H.: Elevation and elevation change of Greenland and Antarctica derived from CryoSat-2, The Cryosphere, 8, 1539–1559, https://doi.org/10.5194/tc-8-1539-2014, 2014.

Holschuh, N., Christianson, K., and Anandakrishnan, S.: Power loss in dipping internal reflectors, imaged using ice-penetrating radar, Annals of glaciology, 55, 49–56, https://doi.org/10.3189/2014AoG67A005, 2014.

Howat, I. M., Porter, C., Smith, B. E., Noh, M.-J., and Morin, P.: The Reference Elevation Model of Antarctica, Cryosphere, 13, 665–674, https://doi.org/10.5194/tc-13-665-2019, 2019.

Jordan, T., Martin, C., Ferraccioli, F., Matsuoka, K., Corr, H., Forsberg, R., Olesen, A., and Siegert, M.: Anomalously high geothermal flux near the South Pole, Scientific reports, 8, 16 785, https://doi.org/10.1038/s41598-018-35182-0, 2018.

Lilien, D. A., Fudge, T., Koutnik, M. R., Conway, H., Osterberg, E. C., Ferris, D. G., Waddington, E. D., and Stevens, C. M.: Holocene Ice-Flow Speedup in the Vicinity of the South Pole, Geophysical Research Letters, 45, 6557–6565, https://doi.org/10.1029/2018GL078253, 2018.

Lindzey, L. E., Beem, L. H., Young, D. A., Quartini, E., Blankenship, D. D., Lee, C.-K., Lee, W. S., Lee, J. I., and Lee, J.: Aerogeophysical characterization of an active subglacial lake system in the David Glacier catchment, Antarctica, The Cryosphere, 14, 2217–2233, https://doi.org/10.5194/tc-14-2217-2020, 2020.

MacGregor, J. A., Winebrenner, D. P., Conway, H. B., Matsuoka, K., Mayewski, P. A., and Clow, G. D.: Modeling englacial radar attenuation at Siple Dome, West Antarctica, using ice chemistry and temperature data, Journal of Geophysical Research: Earth Surface (2003–2012), 112, F03 008, https://doi.org/10.1029/2006JF000717, 2007.

Martos, Y. M., Catalan, M., Jordan, T. A., Golynsky, A., Golynsky, D., Eagles, G., and Vaughan, D. G.: Heat flux distribution of Antarctica unveiled, Geophysical Research Letters, 44, 11 417–11 426, https://doi.org/10.1002/2017GL075609, 2017.

Matsuoka, K., MacGregor, J. A., and Pattyn, F.: Predicting radar attenuation within the Antarctic ice sheet, Earth and Planetary Science Letters, 359, 173–183, https://doi.org/10.1016/j.epsl.2012.10.018, 2012.

Maule, C. F., Purucker, M. E., Olsen, N., and Mosegaard, K.: Heat flux anomalies in Antarctica revealed by satellite magnetic data, Science, 309, 464–467, https://doi.org/10.1126/science.1106888, 2005.

Morlighem, M., Rignot, E., Binder, T., Blankenship, D., Drews, R., Eagles, G., Eisen, O., Ferraccioli, F., Forsberg, R., Fretwell, P., et al.: Deep glacial troughs and stabilizing ridges unveiled beneath the margins of the Antarctic ice sheet, Nature Geoscience, 13, 132–137, https://doi.org/10.1038/s41561-019-0510-8, 2020.

Parrenin, F., Cavitte, M. G. P., Blankenship, D. D., Chappellaz, J., Fischer, H., Gagliardini, O., Masson-Delmotte, V., Passalacqua, O., Ritz, C., Roberts, J., Siegert, M. J., and Young, D. A.: Is there 1.5-million-year-old ice near Dome C, Antarctica?, The Cryosphere, 11, 2427–2437, https://doi.org/10.5194/tc-11-2427-2017, 2017.

Passalacqua, O., Cavitte, M., Gagliardini, O., Gillet-Chaulet, F., Parrenin, F., Ritz, C., and Young, D.: Brief communication: Candidate sites of 1.5 Myr old ice 37km southwest of the Dome C summit, East Antarctica, Cryosphere, 12, 2167–2174, https://doi.org/10.5194/tc-12-2167-2018, 2018.

Peters, M. E., Blankenship, D. D., and Morse, D. L.: Analysis techniques for coherent airborne radar sounding: Application to West Antarctic ice streams, Journal of Geophysical Research: Solid Earth, 110, B06 303, https://doi.org/10.1029/2004JB003222, 2005.

Peters, M. E., Blankenship, D. D., Carter, S. P., Kempf, S. D., Young, D. A., and Holt, J. W.: Along-track focusing of airborne radar sounding data from West Antarctica for improving basal reflection analysis and layer detection, IEEE Transactions on Geoscience and Remote Sensing, 45, 2725–2736, https://doi.org/10.1109/TGRS.2007.897416, 2007.

Price, P. B., Nagornov, O. V., Bay, R., Chirkin, D., He, Y., Miocinovic, P., Richards, A., Woschnagg, K., Koci, B., and Zagorodnov, V.: Temperature profile for glacial ice at the South Pole: Implications for life in a nearby subglacial lake, Proceedings of the National Academy of Sciences, 99, 7844–7847, https://doi.org/10.1073/pnas.082238999, 2002.

Purucker, M.: Geothermal heat flux data set based on low resolution observations collected by the CHAMP satellite between 2000 and 2010, and produced from the MF-6 model following the technique described in Fox Maule et al.(2005), http://websrv.cs.umt.edu/isis/index.php/Antarctica_Basal_Heat_Flux, 2013.

Shapiro, N. M. and Ritzwoller, M. H.: Inferring surface heat flux distributions guided by a global seismic model: particular application to Antarctica, Earth and Planetary Science Letters, 223, 213–224, https://doi.org/10.1016/j.epsl.2004.04.011, 2004.

Siegert, M. J.: On the origin, nature and uses of Antarctic ice-sheet radio-echo layering, Progress in Physical Geography, 23, 159–179, https://doi.org/10.1177/030913339902300201, 1999.

Studinger, M., Medley, B. C., Brunt, K. M., Casey, K. A., Kurtz, N. T., Manizade, S. S., Neumann, T. A., and Overly, T. B.: Temporal and spatial variability in surface roughness and accumulation rate around 88° S from repeat airborne geophysical surveys, The Cryosphere, 14, 3287–3308, https://doi.org/10.5194/tc-14-3287-2020, 2020.

Van Liefferinge, B. and Pattyn, F.: Using ice-flow models to evaluate potential sites of million year-old ice in Antarctica, Climate of the Past, 9, 2335–2345, https://doi.org/10.5194/cp-9-2335-2013, 2013.

Van Liefferinge, B., Pattyn, F., Cavitte, M. G., Karlsson, N. B., Young, D. A., Sutter, J., and Eisen, O.: Promising Oldest Ice sites in East Antarctica based on thermodynamical modelling, The Cryosphere, 12, 2773–2787, https://doi.org/10.5194/tc-12-2773-2018, 2018.

Wessem, J. M. V., Reijmer, C. H., M. Morlighem, J. M., Rignot, E., Medley, B., Joughin, I., Wouters, B., DePoorter, M. A., Bamber, J. L., Lenaerts, J. T. M., van de Berg, W. J., van den Broeke, M. R., and van Meijgaard, E.: Improved representation of East Antarctic surface mass balance in a regional atmospheric climate model, Journal of Glaciology, 60, 761–770, https://doi.org/10.3189/2014JoG14J051, 2014.

Winski, D. A., Fudge, T. J., Ferris, D. G., Osterberg, E. C., Fegyveresi, J. M., Cole-Dai, J., Thundercloud, Z., Cox, T. S., Kreutz, K. J., Ortman, N., et al.: The SP19 chronology for the South Pole Ice Core–Part 1: volcanic matching and annual layer counting, Climate of the Past, 15, 1793—1808, https://doi.org/10.5194/cp-15-1793-2019, 2019.

Winter, A., Steinhage, D., Creyts, T. T., Kleiner, T., and Eisen, O.: Age stratigraphy in the East Antarctic Ice Sheet inferred from radio-echo sounding horizons, Earth System Science Data, 11, 1069–1081, https://doi.org/10.5194/essd-11-1069-2019, 2019.

Winter, K., Ross, N., Ferraccioli, F., Jordan, T. A., Corr, H. F., Forsberg, R., Matsuoka, K., Olesen, A. V., and Casal, T. G.: Topographic steering of enhanced ice flow at the bottleneck between East and West Antarctica, Geophysical Research Letters, 45, 4899–4907, https://doi.org/10.1029/2018GL077504, 2018.

Young, D. A., Lindzey, L. E., Blankenship, D. D., Greenbaum, J. S., De Gorordo, A. G., Kempf, S. D., Roberts, J. L., Warner, R. C., Van Ommen, T., Siegert, M. J., et al.: Land-ice elevation changes from photon-counting swath altimetry: first applications over the Antarctic ice sheet, Journal of Glaciology, 61, 17–28, https://doi.org/10.3189/2015JoG14J048, 2015.

Young, D. A., Roberts, J. L., Ritz, C., Frezzotti, M., Quartini, E., Cavitte, M. G., Tozer, C. R., Steinhage, D., Urbini, S., Corr, H. F., et al.: High-resolution boundary conditions of an old ice target near Dome C, Antarctica, The Cryosphere, 11, 1897–1911, https://doi.org/10.5194/tc-11-1897-2017, 2017.

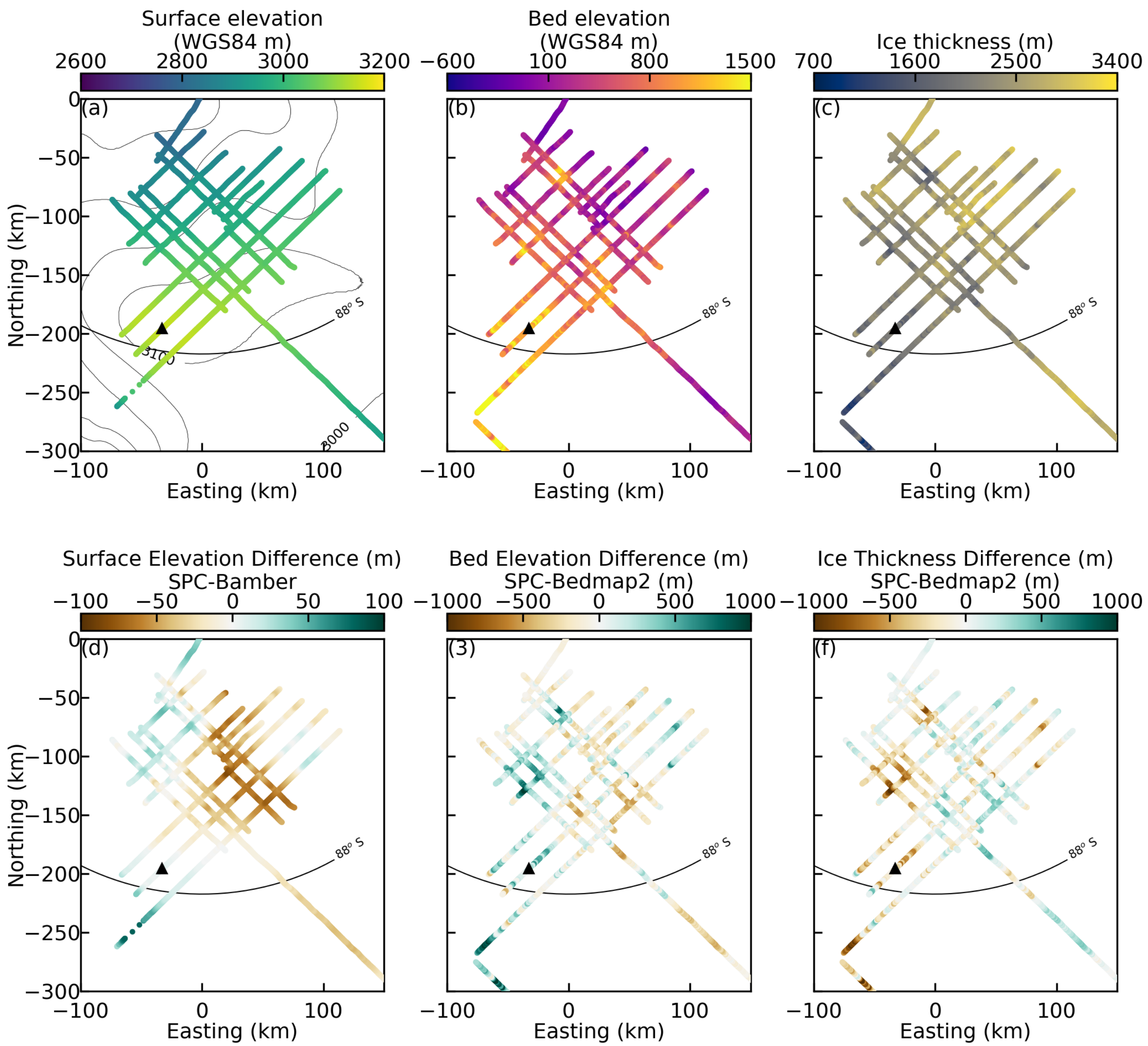

Figure 3. ~~Basic observations~~Geophysically observed ice geometry. (a) ~~Laser~~ is laser surface elevation with background ~~of~~ elevation contours from Bamber et al. (2009) DEM. (~~e~~b) Radar derived bed elevation~~with a background of Bedmap2 (Fretwell et al., 2013)~~. ~~The polygon roughly trace subglacial troughs and are the same as in fig. 5.~~ (~~e~~c) Radar derived ice thickness~~with a background of~~ . (d) Surface elevation difference between the SPC survey and Bamber et al. (2009) DEM. (e) Bed elevation difference between SPC survey and Bedmap2 (Fretwell et al., 2013). (f) Ice thickness difference between the SPC survey and Bedmap2 (Fretwell et al., 2013). The dome summit is marked with a black triangle in each panel. The coordinate system used is polar stereographic (EPSG:3031).

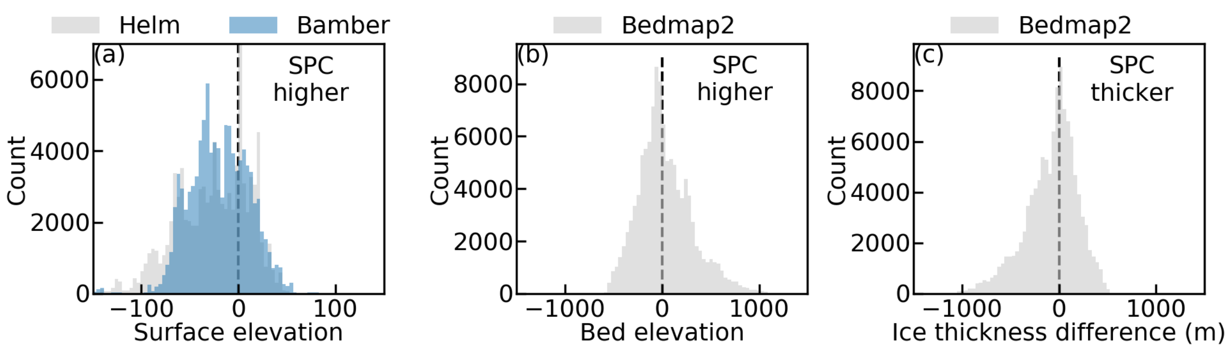

Figure 4. Difference between aerial observations and community DEMs. (a) Laser surface elevation difference ~~from~~ for both Bamber et al. (2009) and Helm et al. (2014), (b) radar bed elevation observation difference from Fretwell et al. (2013), and (c) radar ice thickness observation from Fretwell et al. (2013).

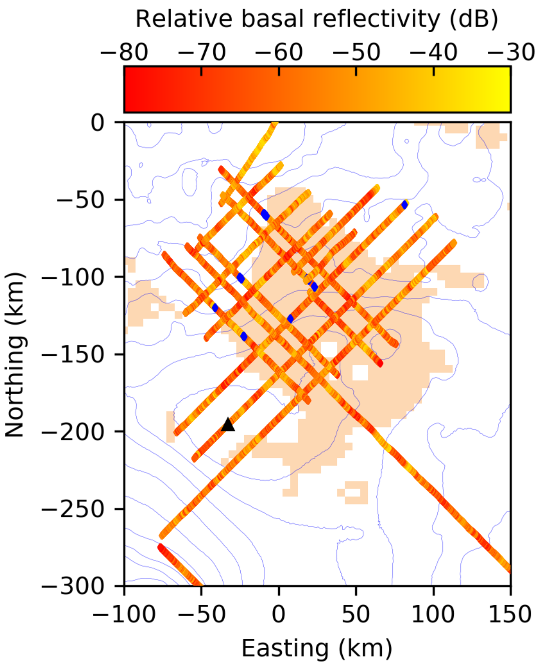

Figure 5. Observed relative basal reflectivity. Reflectivity is corrected for geometric spreading and englacial dielectric attenuation. Locations of reflectivity that exceed -30 dB are ~~highlighted with green squares. The converging subglacial troughs are highlighted with~~ plotted in blue~~polygon and the location the of subglacial mountain is the blue circle~~. Candidate A ice core target region is in orange (Van Liefferinge and Pattyn, 2013). The ~~background~~ dome summit location is plotted as a black triangle. The 500 ~~kPa contours~~ Pa contour intervals are hydraulic potential using Bedmap2 (Fretwell et al., 2013) and zero effective pressure. The highest contour surrounding the dome summit is 29 kPa. The coordinate system used is polar stereographic (EPSG:3031).

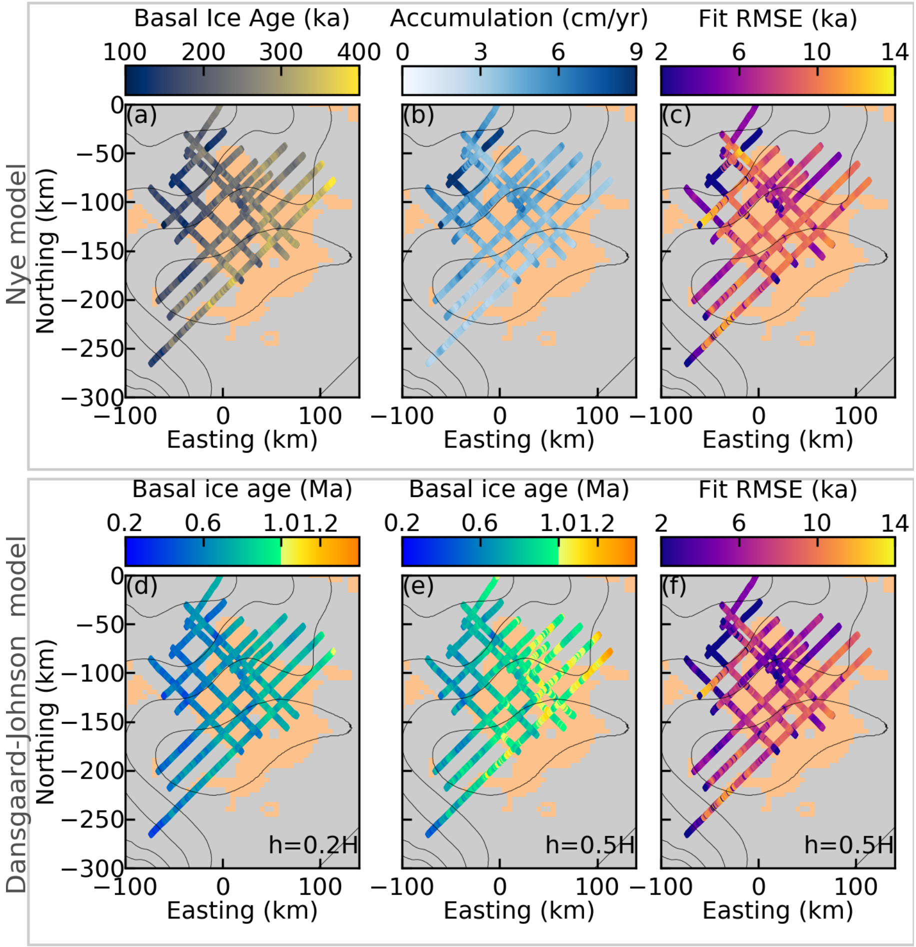

Figure 6. Age model results. The top row are the results of the Nye model and the bottom row the results of the Dansgaard-Johnson model. The RMSE fit is the difference between the model and the dated IRH. Accumulation is reported in ice equivalent units. In panels d, e, and f, h is the characteristic height used in the Dansgaard-Johnson model. Each panel is plotted over candidate A ice core target region in orange (Van Liefferinge and Pattyn, 2013) and 100 m surface elevation contours (Bamber et al., 2009). The dome is surrounded by the 3100 m contour. The coordinate system used is polar stereographic (EPSG:3031).

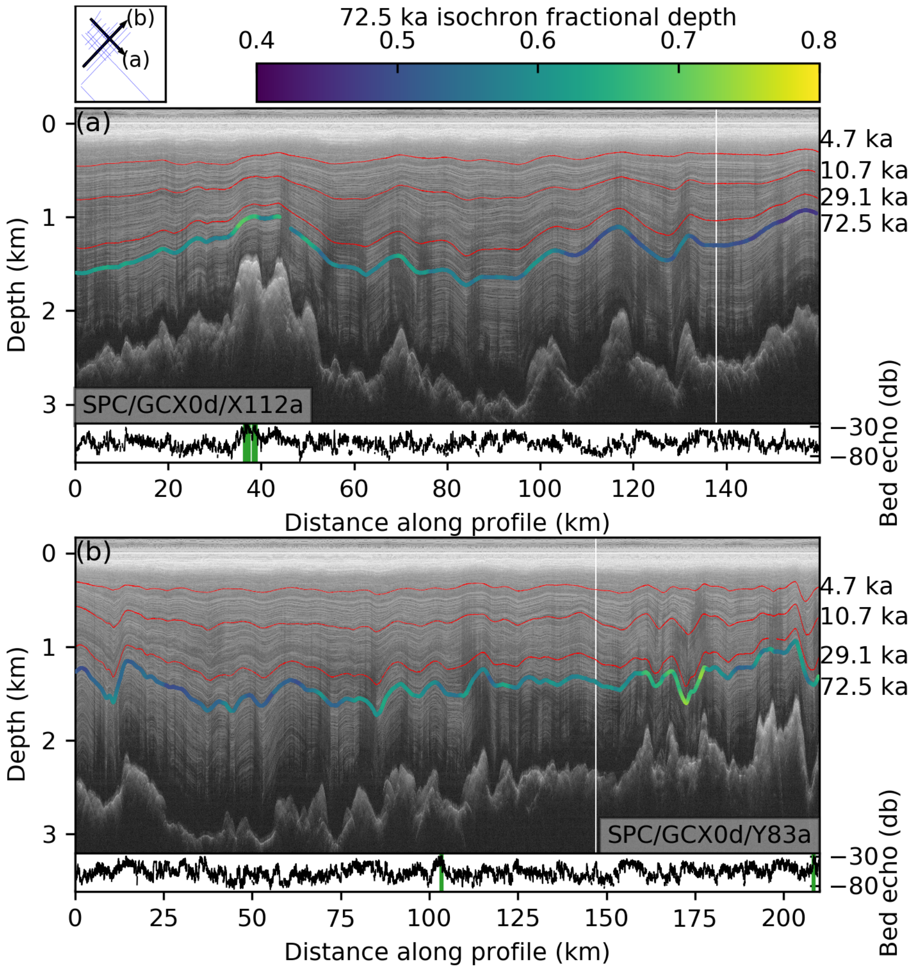

Figure 7. Example radargrams with traced IRH. A context map is in the upper left corner. Beneath each panel is the bed echo strength, which when it exceeds -30 db is highlighted with vertical green lines, the same regions highlighted in Fig. 5. The white vertical line on each radargram represents the intersection of the two transects.

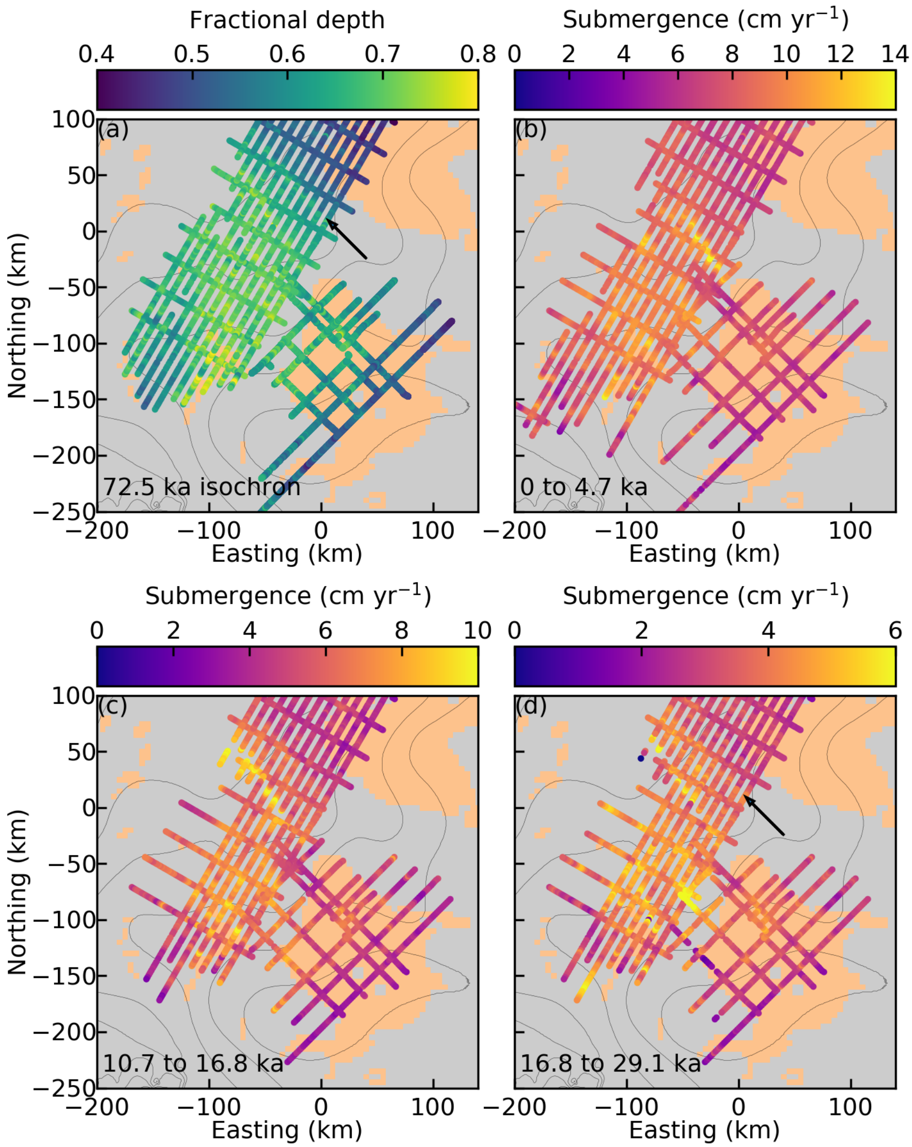

Figure 8. Dated ~~isochron~~ IRH depth and submergence. Panel a is fractional depth of the 72.5 ka IRH. The submergence panels, (b), (c), and (d), show the submergence calculated between ~~the~~ two dated ~~isochrons~~IRH. The black arrow points to and is aligned with a linear feature that marks a boundary of differential IRH drawdown. Each panel is plotted over orange shading, which are ice core target candidates A and B (Van Liefferinge and Pattyn, 2013), and 100 m surface elevation contours (Helm et al., 2014). The dome is surrounded by the 3100 m contour. The coordinate system used is polar stereographic (EPSG:3031).